Original article
DOI: https://doi.org/10.18721/JPM.18104

COMPUTATION OF FLOWS AROUND STATIONARY AND ROTATING CYLINDERS AND A TANDEM OF CYLINDERS AT NEAR-CRITICAL REGIMES USING DDES COUPLED WITH A LAMINAR-TURBULENT TRANSITION MODEL

A. S. Stabnikov✉, *A. V. Garbaruk*

Peter the Great St. Petersburg Polytechnic University, St. Petersburg, Russia

✉ an.stabnikov@gmail.com

Abstract. The objective of this paper is to assess the capabilities of a hybrid RANS-LES approach DDES coupled with algebraic RANS turbulence transition models SST KD and SST alg-γ, allowing the prediction of the laminar-turbulent transition (LTT). The approach is applied to calculations of flows around stationary and rotating cylinders as well as a tandem of stationary cylinders. It is shown that for the simulations of the flows under consideration, this approach significantly outperforms the standard SST DDES (within the standard SST DDES it is assumed that the flow is completely turbulent, and the LTT is not taken into account). At the same time, the obtained computational results depend significantly on the choice of the LTT model, and neither of the two models has a clear advantage in terms of agreement between the computational results and experimental data.

Keywords: turbulence, global hybrid RANS/LES approaches, DDES, drag crisis, Magnus effect

Funding: The reported study was funded by Russian Science Foundation (Grant No. 23-21-00031). http://www.spbstu.ru.

Citation: Stabnikov A. S., Garbaruk A. V., Computation of flows around stationary and rotating cylinders and a tandem of cylinders at near-critical regimes using DDES coupled with a laminar-turbulent transition model, St. Petersburg State Polytechnical University Journal. Physics and Mathematics. 18 (1) (2025) 42–57. DOI: https://doi.org/10.18721/JPM.18104

Научная статья
УДК 532.517.4
DOI: https://doi.org/10.18721/JPM.18104

РАСЧЕТ ОКОЛОКРИТИЧЕСКИХ РЕЖИМОВ ОБТЕКАНИЯ НЕПОДВИЖНОГО И ВРАЩАЮЩЕГОСЯ ЦИЛИНДРОВ И ТАНДЕМА ЦИЛИНДРОВ ПО МЕТОДУ DDES С ПРИВЛЕЧЕНИЕМ МОДЕЛИ ЛАМИНАРНО-ТУРБУЛЕНТНОГО ПЕРЕХОДА

А. С. Стабников✉, *А. В. Гарбарук*

Санкт-Петербургский политехнический университет Петра Великого, Санкт-Петербург, Россия

✉ an.stabnikov@gmail.com

Аннотация. Работа посвящена оценке возможностей вихреразрешающего гибридного RANS-LES-подхода DDES в сочетании с алгебраическими RANS-моделями перехода SST KD и SST alg-γ, описывающими ламинарно-турбулентный переход (ЛТП),

применительно к расчету обтекания неподвижного и вращающегося цилиндров, а также тандема неподвижных цилиндров. Установлено, что при расчете рассмотренных течений этот подход значительно превосходит стандартный SST DDES, в рамках которого ЛТП не учитывается (предполагается, что течение является полностью турбулентным). Наряду с этим, результаты расчетов, полученные с его использованием, существенно зависят от выбора модели ЛТП, и в плане согласования расчета с экспериментом ни одна из двух моделей не имеет явного преимущества.

Ключевые слова: турбулентность, глобальные гибридные RANS/LES-подходы, DDES, кризис сопротивления, эффект Магнуса

Финансирование: Работа выполнена при финансовой поддержке Российского научного фонда (грант № 00031-21-23).

Ссылка для цитирования: Стабников А. С., Гарбарук А. В. Расчет околокритических режимов обтекания неподвижного и вращающегося цилиндров и тандема цилиндров по методу DDES с привлечением модели ламинарно-турбулентного перехода // Научно-технические ведомости СПбГПУ. Физико-математические науки. 2025. Т. 18. № 1. С. 42–57. DOI: https://doi.org/10.18721/JPM.18104

Introduction

With increasing productivity of computing resources, global hybrid RANS-LES approaches have become increasingly popular for engineering calculations; the most well-known and widely used approach is the Delayed Detached Eddy Simulation (DDES) [1]. The accuracy of this, as well as other similar approaches, significantly depends on the computational accuracy of the attached boundary layer, provided by the basic RANS model. In the case when a significant part of the boundary layer is laminar, this accuracy can be radically improved by using basic models that take into account the laminar-turbulent transition (LTT). This is evidenced, in particular, by the results we obtained earlier in [2] for simulation of the flow around a sphere and a cylinder in crossflow at near-critical Reynolds numbers, as well as similar results from [3–8] and others dedicated to simulations crossflow of cylinders, airfoils and turbine blades. It is preferable to use RANS-based LTT models that do not contain additional PDEs for transport of auxiliary quantities responsible for LTT prediction (such models are called algebraic LTT models here and below), so using them practically does not entail an increase in computational costs compared to basic models that do not account for LTT. However, the question of the influence of the specific basic LTT model selected on the accuracy of the resulting solution remains open.

This paper aims to partially clarify this issue by focusing closely on the computational results for near-critical flow regimes of various bluff bodies (stationary cylinder, rotating cylinder, tandem of stationary cylinders) using the DDES method based on two algebraic LTT models: SST KD [2] and SST alg-γ [9].

SST KD DDES and SST alg-γ DDES methods

The formulations of these approaches are based on the equations of the semi-empirical k-ω SST RANS turbulence model [10]. In both cases, the PDE for transport of specific turbulence dissipation ω of the SST model remains unchanged, and all its modifications aimed at accounting for LTT are related to the equation for transport of turbulence kinetic energy k, which can be written as follows within the approaches applied:

$$\frac{\partial(\rho k)}{\partial t}+\frac{\partial\left(\rho u_i k\right)}{\partial x_i}=\gamma P_k+P_{\text{bubble}}-\frac{\beta^*\rho\omega k^{3/2}}{l_{\text{DDES}}}+\frac{\partial}{\partial x_i}\left[\left(\mu+\sigma_k\mu_t\right)\frac{\partial k}{\partial x_i}\right], \quad (1)$$

where ρ is the density; μ, μ_t are the dynamic coefficients of molecular and turbulent viscosities; x_i are the components of the coordinate system; u_i are the components of velocity; σ_k, β^* are the constants of the SST model; P_k is the generation term.

The turbulence length scale l_{DDES} is a combination of the turbulence length scale of the SST model

$$l_{\text{RANS}} = k^{1/2}/\beta^*\omega$$

and the subgrid-scale length scale $\Delta_{\text{SLA}}^{\text{DDES}}$, adapted to the mixing layers [11]; l_{DDES} is calculated by the formula presented in [1]:

$$l_{\text{DDES}} = l_{\text{RANS}} - f_d \max\{0, (l_{\text{RANS}} - C_{\text{DES}}\Delta_{\text{SLA}}^{\text{DDES}})\}, \tag{2}$$

where is the shielding function f_d, defined as

$$f_d = 1 - \tanh\left[\left(C_{d1} r_d\right)^{C_{d2}}\right], r_d = \left(\nu_{\text{t}} + \nu\right) \Big/ \left(\kappa^2 d_w{}^2 \sqrt{0.5 \cdot \left(S^2 + \Omega^2\right)}\right) \tag{3}$$

ensures DDES operation in RANS regime in the entire attached boundary layer.

The quantities included in Eq. (3) are defined as follows: ν_t, ν are the kinematic coefficients of turbulent and molecular viscosities; d_w is the distance from the point under consideration to the nearest wall; S, Ω are the magnitudes of strain rate and vorticity tensors; empirical constants have the following values:

$$C_{\text{DES}} = F_1 \cdot C_{\text{DES1}} + (1 - F_1) \cdot C_{\text{DES2}},$$

$$C_{\text{DES1}} = 0.78,\ C_{\text{DES2}} = 0.61,\ C_{d1} = 20.0,\ C_{d2} = 3.0,\ \kappa = \text{•}\,,41,\ \beta^* = 0.09,$$

where F_1 is a function of the SST model [10], which is a boundary layer detector.

The values given coincide with the values of the corresponding constants of the SST DDES method [1].

The additional terms introduced in Eq. (1) (compared with the standard equation for transport of k of the SST model) to account for LTT, namely, the intermittency γ and the generation term P_{bubble}, intended to describe the separation ('bubble') transition, are found by the same formulas as in the SST KD [2] or SST alg-γ [9] RANS models of the LTT. However, since these terms should function only in the RANS region of DDES, these terms are deactivated in the regions where the value of the weighting function F_1 of the SST model satisfies the condition $F_1 < 0.9$ (i.e., outside the RANS region), that is, the value of γ is assumed to be equal to 1, and the value of P_{bubble} is assumed to be equal to zero.

Problem statement

To assess the influence of the LTT model on the accuracy of the DDES method based on it, three flows were selected where LTT plays a key role.

The first of these is the crossflow of a stationary cylinder in a wide range of Reynolds numbers, including subcritical, critical and subcritical regimes. Study of this problem allows to evaluate the capability of eddy-resolving approaches to predict the drag crisis phenomenon.

The second flow is crossflow over a rotating cylinder (Fig. 1, *a*) under regimes characterized by the so-called inverse Magnus effect. The direct Magnus effect is widely known. It consists in the occurrence of a lift force induced by an increase in pressure in the vicinity of the lower part of the cylinder moving upstream and a decrease in pressure in the vicinity of its upper part moving downstream (the cylinder is assumed to rotate clockwise and the flow is directed from left to right). However, with a certain combination of the rotational velocities of the cylinder and the Reynolds numbers, a change in the direction of the lift force is observed in experiments, which is called the inverse Magnus effect. It is caused by the LTT in the boundary layer on the lower side of the cylinder, which leads to displacement of the separation downstream and a corresponding decrease in local pressure. LTT does not occur on the upper surface of the cylinder, with laminar separation observed, therefore the pressure is higher than on the lower surface. These specific modes are considered in the paper.

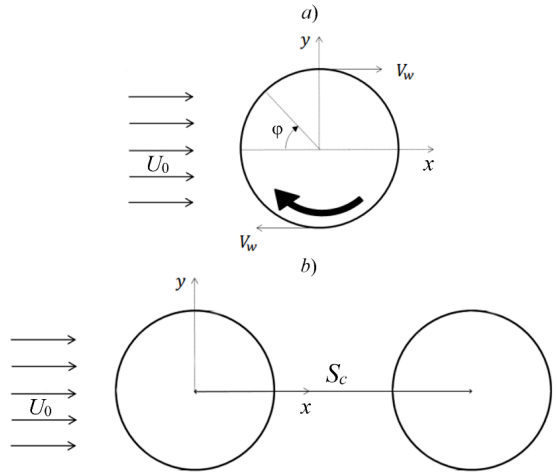

Fig. 1. Schematic of two flows considered: flow around rotating circular cylinder (*a*) and tandem of stationary cylinders (*b*); V_w is the linear rotational velocity of the cylinder wall, S_c is the distance between the cylinder axes
Thin arrows indicate the direction of the free stream (U_0 is its velocity)

The third flow considered is the crossflow over a tandem of stationary cylinders (Fig. 1,*b*), which was studied in detail in the experimental work [12]. Depending on the distance between the cylinders S_c and the Reynolds number Re, three characteristic regimes can be distinguished [12], illustrated in Fig. 2 for $S_c/D = 2.8$ (S_c/D is the dimensionless distance between the cylinders in the tandem, D is the cylinder diameter).

In the first regime, subcritical flow around the front cylinder of the tandem is observed, LTT occurs in the separated mixing layer, and a global (without forming a Kármán vortex street) separation region with low pressure is formed between the cylinders, which entails low or even negative drag of the rear cylinder of the tandem. With this type of flow, a single vortex street is formed behind the cylinders, shown in Fig. 2 in blue.

The second regime corresponds to supercritical flow around the front cylinder, where a pronounced Kármán vortex street is formed in its wake, and the width of the wake is significantly reduced. In this case, the drag of the rear cylinder becomes higher than that of the front cylinder, and a separate Kármán vortex street is formed in its wake (shown in green in Fig. 2).

With a further increase in the Reynolds number (transcritical flow), the wake behind the first cylinder gradually expands, which is accompanied by an increase in its drag and a decrease in the drag of the second cylinder.

Thus, accurately determining the LTT position for flow around the front cylinder of the tandem is critically important for determining the drag of the rear cylinder.

The values of the governing parameters of the three flows described above, namely the Reynolds number $\mathrm{Re} = U_0 D/\nu$, based on the diameter of the cylinder D and the freestream velocity U_0, the relative rotational velocity of the cylinder $\alpha = V_w/U_0$ (V_w is the linear rotational velocity of the cylinder wall) and the dimensionless distance between the cylinders of the tandem S_c/D are given in Table 1.

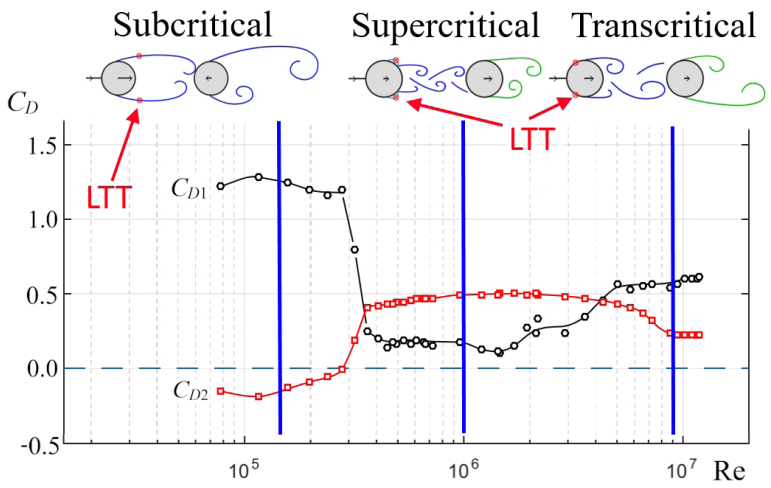

Fig. 2. Experimental dependences of drag for front (C_{D1}) and rear (C_{D2}) cylinders in the tandem on Re at $S_c/D = 2.8$ [12]; scheme of three flow regimes: subcritical, supercritical and transcritical; LTT is the laminar-turbulent transition
The vertical lines correspond to the three values of the Reynolds number considered in this paper

The computational domain for the flow around the single cylinder (both stationary and rotating) is a cylinder with a radius of $25D$ and centered at the point $(x,y) = (0,0)$ coinciding with the center of the cylinder (the flow is in the positive direction of the x axis). The computational domain for the flow around the tandem of cylinders is a rectangular parallelepiped, whose height $L_y/D = 10$ is equal to the height of the wind tunnel in the experiment [12], and the x coordinate varies from $-20.0D$ to $+27.3D$.

Table 1

Main computational parameters of three selected flows and their values

Body in crossflow	Re, 10^5	2nd parameter
Stationary single cylinder	0.5–9.0	–
Rotating single cylinder	3.65	$0 \le \alpha \le 0.6$
Tandem of stationary cylinders	1.5; 10.0; 80.0	$S_c/D = 2.8; 4.0$

Notations: Re is the Reynolds number equal to U_0D/ν, constructed from the diameter of the cylinder D and the freestream velocity U_0 (ν is the molecular viscosity); α is the relative rotational velocity of the cylinder equal to V_w/U_0 (V_w is the linear rotational velocity of the cylinder wall); S_c/D is the dimensionless distance between the tandem cylinders.

All velocity components were set to zero on the surface of the stationary cylinder, and assumed to be equal to the components of the local surface velocity on the surface of the rotating cylinder. The pressure gradient normal to the wall and the turbulence kinetic energy k were assumed to be zero, and its specific dissipation rate ω was calculated by the formula recommended in [13]:

$$\omega_W = \frac{60\nu}{\beta_1 (\Delta d_1)^2}, \tag{4}$$

where β_1 is the constant of the SST model, $\beta_1 = 0.075$; Δd_1 is the size of the first near-wall step of the mesh.

Table 2

Boundary conditions for turbulent characteristics at inlet boundary

Streamlined body	Re, 10^5	Boundary value	
		k/U_0^2, 10^{-4}	$\omega D/U_0$
Stationary circular cylinder	0.5	0.240	4.0
	1.3	0.614	10.9
	1.7	0.799	24.3
	2.5	1.350	42.8
	3.0	1.500	47.9
	4.0	1.560	49.9
	5.0	1.980	64.0
	7.0	2.730	88.6
	9.0	3.600	11.8
Rotating circular cylinder	3.65	1.380	4.78
Tandem of stationary cylinders	1.5	1.220	20.3
	10.0	6.000	120
	80.0	9.380	174

Notation: Re is the Reynolds number, k/U_0^2 is the normalized turbulence kinetic energy, $\omega D/U_0$ is the normalized specific velocity of dissipation k.

Table 3

Selected turbulence intensities Tu in the vicinity of streamlined cylinders

Streamlined body	Tu, %
Stationary circular cylinder	0.30 [14]
Rotating circular cylinder	0.90 [15]
Tandem of stationary cylinders	0.45 [12]

Note. The values of Tu in the vicinity of the streamlined cylinders were expected to coincide with the corresponding values in [14, 15, and 12].

Constant values of velocity $u = U_0$, turbulence kinetic energy k and its specific dissipation rate ω were set at the inlet boundary of the computational domain (Table 2). These values were selected in such a way that when they were fixed in the region $x \le -2.0D$ and calculated further downstream, the turbulence intensities $\mathrm{Tu} = 100 \cdot \overline{u'^2} / U_0$ in the vicinity of the streamlined cylinders coincided with the corresponding values in [14, 15, 12] (Table 3).

Finally, the pressure at the inlet boundary was determined by linear extrapolation of its values from the internal points of the computational domain.

In addition, the conditions of free slip ('symmetry') were set for simulation of flow around the tandem cylinders at the upper and lower boundaries of the computational domain.

As for the boundary conditions along the transverse z coordinate, it was assumed for all flow simulations that they were statistically homogeneous in the transverse direction z ('quasi-two-dimensional'). For this reason, periodic boundary conditions were imposed at the lateral boundaries of the computational domain, whose size in the direction z was $L_z = 5D$ in all simulations (this is slightly greater than the width the computational domain πD, typically used in simulations of cylinder flow in the quasi-two-dimensional approximation (see, for example, [16, 17])).

As an initial approximation, homogeneous fields with values equal to the values of the corresponding quantities at the inlet boundary of the computational domain were set for all required variables, except pressure, and the pressure was assumed in the initial approximation to be equal to the pressure at the outlet boundary.

The flow around a single cylinder was simulated using O-type meshes with clustering in the attached boundary layer and in the wake behind the cylinder. Three such meshes were built, containing 56, 65 and 73 million cells, differing in the magnitude of the first near-wall step in the radial direction to ensure that the condition $\Delta d_1^+ < 1$ was satisfied in all simulations. The mesh with 56 million cells satisfies this condition at the value of $\mathrm{Re} < 10 \cdot 2.5^5$, the mesh with 65 million cells at $\mathrm{Re} < 6.0 \cdot 10^5$, and the mesh with 73 million cells at $\mathrm{Re} < 1.0 \cdot 10^6$. Selective simulations with refined meshes indicate that the constructed meshes ensure grid independence of time-averaged solutions.

The average of the constructed meshes (65 million cells) was used for all simulations of the flow around the rotating cylinder.

The step sizes of the computational meshes used for simulations of the flow around the tandem of cylinders approximately coincided with the step sizes of the most refined mesh for a single cylinder (73 million cells), and the number of cells in these meshes was 86 and 89 million for $S_c/D = 2.8$ and 4.0, respectively.

The time integration step was $\Delta t = 10 \cdot 5^{-3} D/U_0$, providing the Courant number CFL < 1 in the separation zone in the wake behind the cylinders. The simulations were run over a time interval of about $100 \cdot D/U_0$. A statistically steady solution was achieved in the first half of the time interval, and nonstationary data were accumulated in the second half to compute time-averaged characteristics of the flow.

Computational aspects

All results presented below were obtained with the in-house academic finite-volume code NTS [18], using multi-block structured overset meshes (Chimera technology), allowing to perform simulations of geometrically complex flows with higher-order approximation schemes.

Incompressible flows studied in this paper were simulated with the NTS code using the Rogers–Kwak method for flux-difference splitting [19], combining the scheme for flux vector splitting of gas dynamic equations and the Yanenko–Chorin method for introducing artificial compressibility [20].

The method for approximating the inviscid components of the flux vectors in the equations of motion, determining the dissipative properties of the scheme plays an important role within the framework of hybrid RANS-LES approaches; the requirements for this method vary in different regions of the flow. The scheme should ensure the stability of the solution on relatively coarse anisotropic meshes in the RANS region, which is achieved by using excessively dissipative upwind-biased schemes. In contrast, it is necessary to use less-dissipative schemes providing resolution of small-scale turbulence in LES regions. The boundary between RANS and LES regions is determined automatically during the solution process in global hybrid approaches, including the DDES method, which, in general, does not allow to explicitly prefer a specific scheme in certain regions of the computational domain. In such cases, it is common to use a combination of selected schemes with a space-variable weight, determined during the solution process. A hybrid scheme was used in this work to determine the weights of a third-order upwind scheme and a fourth-order central difference scheme [21].

The inviscid components of the flux vectors in the equations for transport of k and ω were approximated using a second-order upwind scheme. The viscous components of the flux vectors in all equations were approximated using a second-order central difference scheme. An implicit three-layer second-order Euler scheme was used to approximate the time derivatives [22]. In this case, 20 internal iterations in pseudo-time were performed at each time step.

To solve the system of discrete analogues of the initial gas dynamic equations, Gauss–Seidel plane relaxation was used at each iteration, and the transport equations of turbulent characteristics were solved using a modified (with diagonal predominance) method of approximate factorization in spatial directions.

The simulations were parallelized via the hybrid MPI/Open-MP concept, making it possible to ensure efficient operation of the program on computers with both distributed and shared or combined RAM.

Computational results and analysis

Flow around stationary circular cylinder. Fig. 3 shows the distributions of the time-averaged skin friction and pressure drag C_f and C_p at different Reynolds numbers, obtained from simulations using the standard (not taking into account LTT) SST DDES method and its two versions taking into account LTT.

Judging from these distributions, the standard SST DDES predicts turbulent separation over the entire variation range of the Reynolds number under consideration, and the results obtained using it differ significantly from the corresponding results obtained using the SST KD DDES and SST alg-γ DDES methods taking into account LTT.

The results obtained using these methods accounting for LTT depend significantly on the Reynolds number.

In particular, both methods predict similar distributions C_f and C_p at $\mathrm{Re} = 1.3 \cdot 10^5$, typical for subcritical flow regimes characterized by laminar separation.

If the Reynolds number is close to the critical value ($\mathrm{Re} = 2.5 \cdot 10^5$), the C_f and C_p distributions obtained using SST KD DDES and SST alg-γ DDES differ greatly from each other. The first of these methods predicts the subcritical nature of the flow, as can be judged by the pressure distribution over the surface, and the second is subcritical, with a bubble transition.

At $\mathrm{Re} = 4 \cdot 10^5$, the distributions C_f and C_p obtained using methods accounting for LTT become close again and resemble the distributions observed in supercritical flow regime with bubble LTT.

Finally, at $\mathrm{Re} = 9 \cdot 10^5$, the results of both models are also close to each other and (as should be the case with significantly supercritical flow regimes) are characterized by LTT in the attached boundary layer and separation of the turbulent boundary layer.

All the described characteristics of the C_f and C_p distributions are reflected in the computational dependences of drag.

$$C_D = F_x \Big/ \left[\left(\tfrac{1}{2} \right) \rho U_0^2 L_z D \right]$$

(F_x is the total drag force acting on the cylinder) on the Reynolds number (Fig. 4).

Fig. 4 also shows experimental data [14, 23–25].

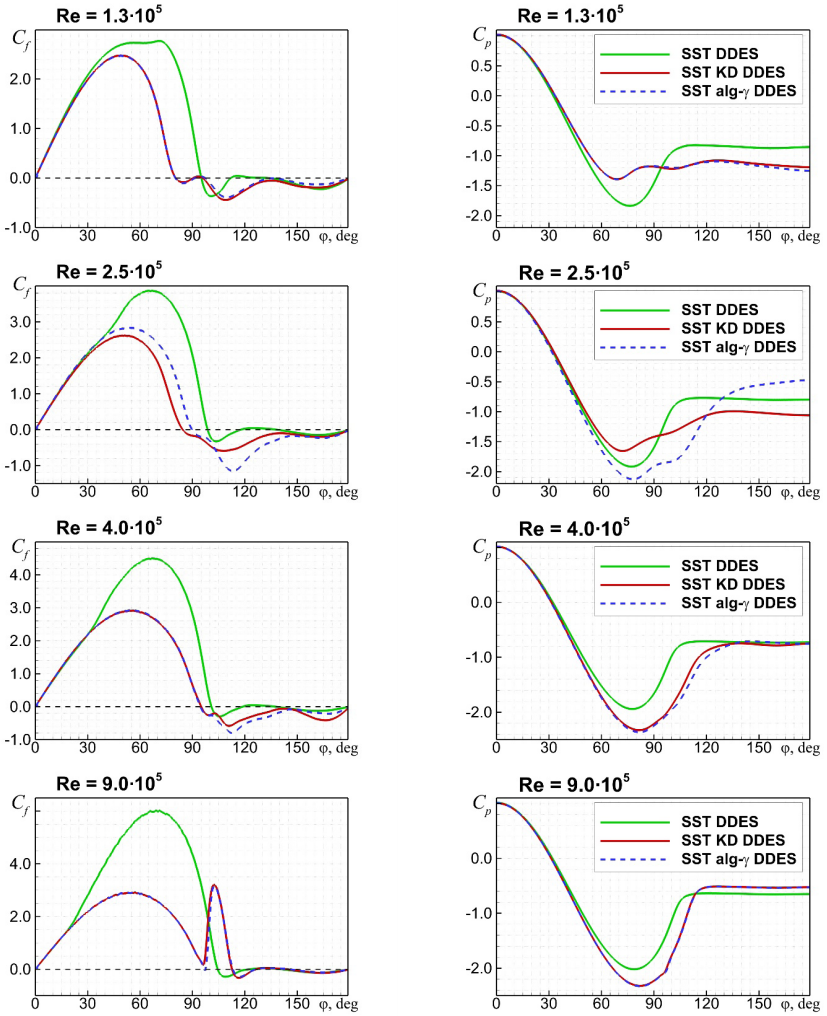

Fig. 3. Comparison of computational dependences of skin friction drag C_f and pressure drag C_p (averaged over time and transverse direction) on polar angle obtained using three methods at Re $1.3 \cdot 10^5$; $2{,}5 \cdot 10^5$; $4.0 \cdot 10^5$ and $9.0 \cdot 10^5$

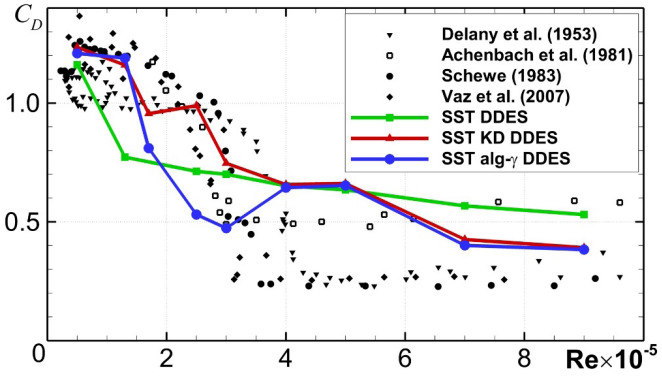

Fig. 4. Computational dependences of cylinder drag on Reynolds number, obtained by three methods: comparison with experimental data

In particular, unlike the original SST DDES method, both approaches that take into account LTT describe the drag crisis qualitatively correctly (a sharp drop in C_D at Reynolds numbers in the vicinity of Re = $1.5 \cdot 10^5$). In addition, for subcritical (Re < $1.5 \cdot 10^5$) and significantly supercritical (Re > $7.0 \cdot 10^5$) Reynolds numbers, drag does not depend on the LTT model used and agrees well with experimental data (which vary widely).

However, in the range of Reynolds numbers $1.3 \cdot 10^5$ < Re < $10 \cdot 4.0^5$, there is a significant difference in the C_D(Re) dependence obtained using the SST KD DDES and SST alg-γ DDES methods, and, unlike in the experiment, their nonmonotonic variation.

Finally, with a further increase in the Reynolds number, the computational results using both models become close again, but at Re < $7.0 \cdot 10^5$ they differ significantly from the measurement results.

In general, the results obtained indicate that none of the methods provides a satisfactory description of the flow around the cylinder with a bubble LTT. The reasons for this remain unclear. However, it can be assumed that this is due to the insufficiently rapid growth of turbulent viscosity in the separation bubble. Notably, no such phenomenon is observed in the computational results for flow around a sphere [26]. This indirectly indicates that it is at least partially related to the effect of strong large-scale oscillations of the cylinder's near wake on the separation bubble.

Flow around rotating cylinder. For the considered values of the Reynolds number and the dimensionless rotational velocity of the cylinder (Re = $3.65 \cdot 10^5$, $0 \le \alpha \le 0.6$), accounting for LTT led to a qualitative change in the distribution of time-averaged pressure drag C_p over its surface (Fig. 5).

Thus, the SST DDES method, which does not account for LTT, predicts a monotonic increase in the flow asymmetry relative to the $y = 0$ plane as the rotational velocity increases: pressure decreases on the upper surface and increases on the lower surface, which leads to a monotonic increase in the Magnus effect (an increase in lift force).

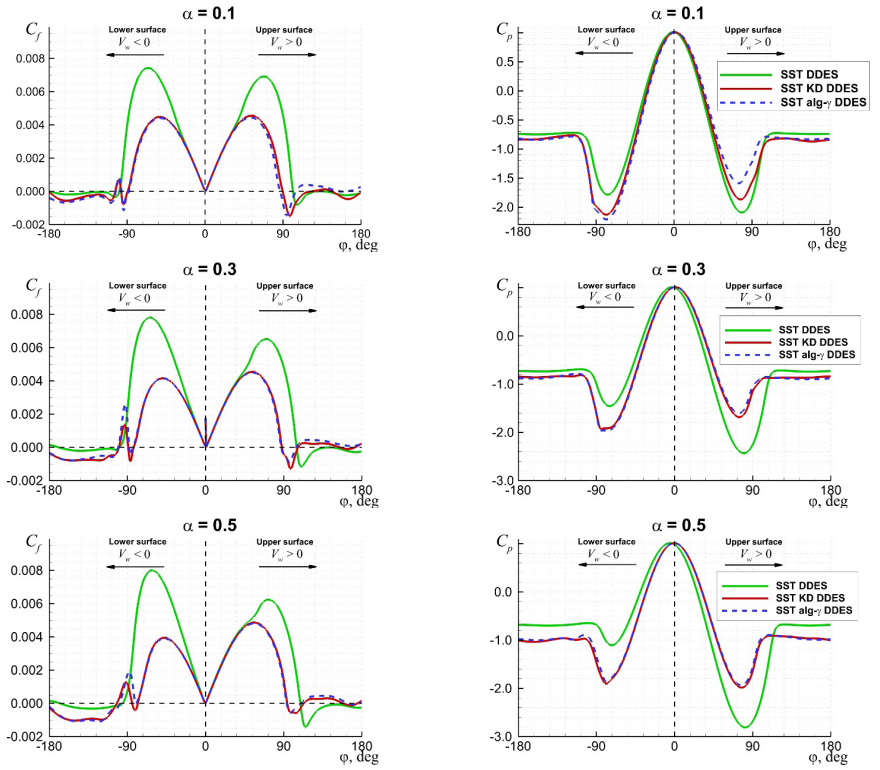

Fig. 5. Computational polar distributions of skin friction drag C_f and pressure drag C_p (averaged over time and transverse direction) over the lower and upper surfaces of rotating cylinder at different relative rotational velocities α

(reference point of the polar angle φ is shown in Fig. 1,*a*; V_w is the linear rotational velocity of the cylinder wall)

In contrast, both DDES versions used, which account for LTT, predict a different type of separation on the two sides of the cylinder, namely laminar on the upper surface and turbulent on the lower surface. The turbulent separation is shifted downstream relative to the laminar one, which leads to a certain decrease in pressure on the lower surface relative to the upper surface, which exceeds its increase at $\alpha < 0.5$ due to rotation. Data related to the friction drag C_f are also presented.

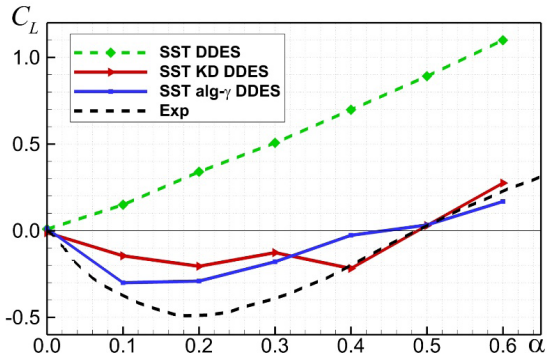

Fig. 6. Computational dependences of lift in rotating cylinder on relative rotational velocity α, obtained using three methods: comparison with experimental data [27]

As a result, the lift force turns out to be negative at $0 < \alpha < 0.5$ in the solutions obtained using the SST KD DDES and SST alg-γ DDES methods, i.e., both methods describe the inverse Magnus effect (Fig. 6). The value of the lift force C_L predicted by the SST DDES method is positive and increases monotonically with increasing rotational velocity.

A comparison of the computational and experimental dependences of $C_L(\alpha)$ shown in Fig. 6 indicates that the SST KD DDES and SST alg-γ DDES methods accurately predict the variation range of rotational velocity α, where the inverse Magnus effect is observed, however, they somewhat underestimate the magnitude of the negative lift force compared with the experimental value. The quantitative difference between the dependences predicted by different methods accounting for LTT turns out to be rather significant, however, the same as for a stationary cylinder, it is difficult to give preference to any of the models in this case. For example, the results obtained using SST alg-γ DDES are in better agreement with experimental data at $\alpha \le 0.3$, and the results obtained using SST KD DDES are in better agreement with experimental data at $\alpha > 0.3$.

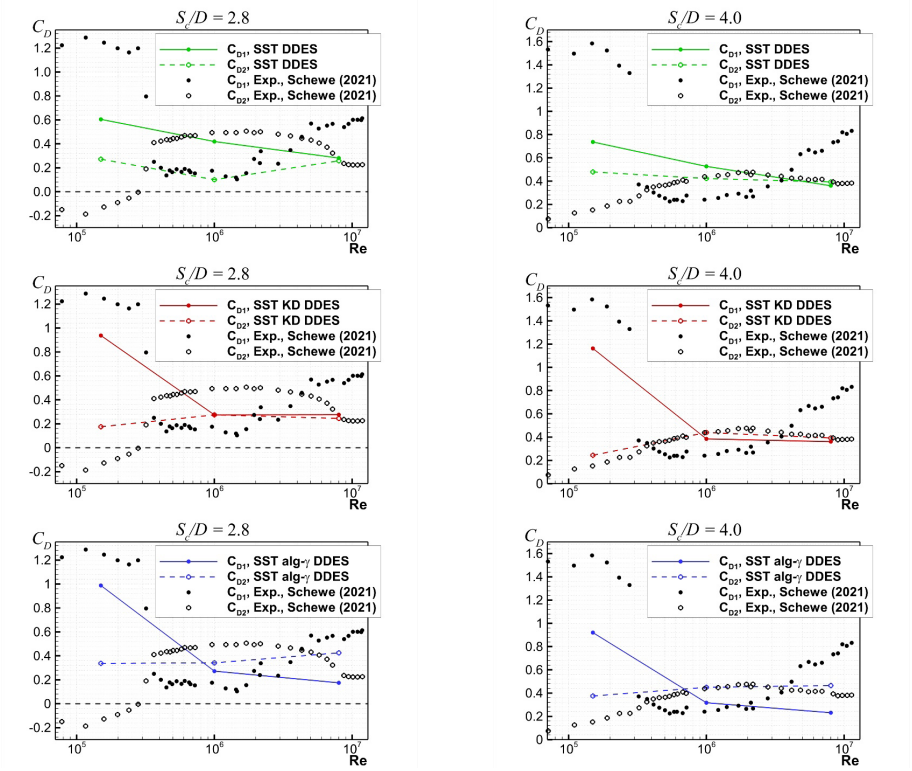

Fig. 7. Computational dependences of drag for front (C_{D1}) and rear (C_{D2}) tandem cylinders on Reynolds number: comparison with experimental data [12]

Flow around tandem of cylinders. Computational results for this flow are shown in Fig. 7. As for the two flows discussed above, DDES versions accounting for LTT seem superior over the standard SST DDES method. For example, according to measurements, under the subcritical flow regime of the first cylinder ($\mathrm{Re} = 1.5 \cdot 10^5$), its drag is much higher than that of the second cylinder (the latter turns out to be negative at $S_c/D = 2.8$). Among the three methods considered, the SST KD DDES method predicts the greatest difference between the drag of the first and second cylinders, however, in this case this difference turns out to be significantly less than that observed in the experiment.

As noted earlier (see the section 'Problem statements'), the drag of the second cylinder exceeds the drag of the first in subcritical regime ($\mathrm{Re} = 1 \cdot 10^6$). For both considered distances S_c/D, this effect is predicted only by the SST alg-γ DDES method, and for SST KD DDES, it is observed only at $S_c/D = 4.0$ (according to this method, the drag coefficients of both cylinders turn out to be almost equal at $S_c/D = 2.8$). The difference between the drag of the rear and front cylinders is underestimated in all cases. The standard SST DDES method predicts a qualitatively incorrect result: the drag of the first cylinder exceeds the drag of the second.

Finally, the drag of the first cylinder again becomes higher than the drag of the second in transcritical regime ($\mathrm{Re} = 8 \cdot 10^6$). This effect is not predicted by any of the three methods, and SST alg-γ DDES predicts a qualitatively incorrect result, and according to the other two methods, the drag coefficients of both cylinders are almost equal.

Thus, the same as in the first two problems, both versions of DDES, which take into account LTT, significantly exceed the SST DDES method in accuracy. The error of the solutions obtained using these methods remains very high, and it is not possible to give preference to any of these versions of DDES.

Conclusion

The example of three separation flows (crossflow over stationary and rotating single cylinders and tandem of stationary cylinders), where the laminar-turbulent transition (LTT) plays a major role, was used for detailed analysis of the potential of the eddy-resolving hybrid RANS-LES approach DDES SST combined with algebraic LTT models (SST KD or SST alg-γ) for simulations of these flows. We established that in all the cases considered, both methods that take into account LTT allow to describe the drag crisis phenomenon, in contrast to the standard DDES version with the basic SST RANS model. The choice of the LTT model has a significant impact on the computational results, especially in near-critical flow regimes. However, it is impossible to select either of the two LTP models considered once and for all, since both of them turn out to be accurate in different cases.

The simulations were run on the Polytechnic RSC Tornado cluster of the Polytechnic Supercomputer Center (http://www.scc.spbstu.ru).

REFERENCES

1. **Spalart P. R., Deck S., Shur M. L., et al.,** A new version of Detached-Eddy Simulation, resistant to ambiguous grid densities, Theor. Comput. Fluid Dyn. 20 (3) (2006) 181–195.

2. **Stabnikov A. S., Garbaruk A. V.,** An algebraic transition model for simulation of turbulent flows based on a Detached Eddy Simulation approach, St. Petersburg Polytechnical State University Journal. Physics and Mathematics. 15 (1) (2022) 16–29 (in Russian).

3. **Sшrensen N. N., Bechmann A., Zahle F.,** 3D CFD computations of transitional flows using DES and a correlation based transition model, Wind Energy. 14 (1) (2011) 77–90.

4. **Hodara J., Smith M. J.,** Improved turbulence and transition closures for separated flows, Proc. 41st Eur. Rotorcraft Forum (ERF2015-113). 1-st–4-th Sept., Munich, Germany (2015) 18.

5. **Kim H. J., Kwon O. J.,** Numerical simulation of transitional flows using a blended IDDES and correlation-based transition model, Comput. Fluids. 222 (30 May) (2021) 104916.

6. **You J. Y., Kwon O. J.,** A blended model for simulating massive flow separation and laminar–turbulence transition, Proc. 42nd AIAA Fluid Dynamics Conference and Exhibit. 25–28 June, 2012. New Orleans, Louisiana, USA, AIAA (2012) 2971.

7. **Sa J. H., Park S. H., Kim C. J., Park J. K.,** Low-Reynolds number flow computation for eppler 387 wing using hybrid DES/transition model, J. Mech. Sci. Technol. 29 (5) (2015) 1837–1847.

8. **Coder J. G., Ortiz-Melendez H. D.,** Transitional Delayed Detached-Eddy Simulation of multielement high-lift airfoils, J. Aircr. 56 (4) (2019) 1303–1312.

9. **Menter F. R., Matyushenko A., Lechner R., et al.,** An algebraic LCTM model for laminar–turbulent transition prediction, Flow Turbul. Combust. 109 (4) (2022) 841–869.

10. **Menter F. R., Kuntz M., Langtry R.,** Ten years of industrial experience with the SST turbulence model, Heat Mass Transf. 2003. Vol. 4 (Jan) (2003) 1–9.

11. **Probst A., Schwamborn D., Garbaruk A., et al.,** Evaluation of grey area mitigation tools within zonal and non-zonal RANS-LES approaches in flows with pressure induced separation, Int. J. Heat Fluid Flow. 68 (Dec) (2017) 237–247.

12. **Schewe G., van Hinsberg N. P., Jacobs M.,** Investigation of the steady and unsteady forces acting on a pair of circular cylinders in crossflow up to ultra-high Reynolds numbers, Exp. Fluids. 62 (8) (2021) 176.

13. **Menter F. R.,** Two-equation eddy-viscosity turbulence models for engineering applications, AIAA J. 32 (8) (1994) 1598–1605.

14. **Schewe G.,** On the force fluctuations acting on a circular cylinder in crossflow from subcritical up to transcritical Reynolds numbers, J. Fluid Mech. 133 (Aug) (1983) 265–285.

15. **Zheng Z., Lei J., Wu X.,** Numerical simulation of the negative Magnus effect of a two-dimensional spinning circular cylinder, Flow Turbul. Combust. 98 (1) (2017) 109–130.

16. **Pereira F. S., Vaz G., Eza L.,** An assessment of Scale-Resolving Simulation models for the flow around a circular cylinder, Proc. Eighth Int. Symp. on Turbulence Heat and Mass Transfer (THMT-15). 14-th Sept., 2015. Sarajevo, Bosnia and Herzegovina: Begell House, USA (2015) 295–298.

17. **Pereira F. S., Vaz G., Eza L.,** Flow past a circular cylinder: A comparison between RANS and hybrid turbulence models for a low Reynolds number, Proc. ASME 2015 34th Int. Conf. on Ocean, Offshore and Arctic Engineering, Vol. 2: CFD and VIV, May 31–June 5, 2015. St. John's, Newfoundland, Canada: ASME (2015) V002T08A006.

18. **Shur M., Strelets M., Travin A.,** High-order implicit multi-block Navier–Stokes code: Ten-year's experience of application to RANS/DES/LES/DNS of turbulent flows (Invited lecture), Proc. 7th Symp. on Overset Composite Grids and Solution Technology, Oct. 5–7, 2004, Huntington Beach, USA (2004). https://cfd.spb.ru/agarbaruk/doc/NTS_code.pdf

19. **Rogers S., Kwak D.,** An upwind differencing scheme for the time-accurate incompressible Navier–Stokes equations, Proc. 6th Applied Aerodyn. Conf. June 06–08, 1988. Williamsburg, USA.: American Institute of Aeronautics and Astronautics (AIAA) (1988) 88-2583-CP.

20. **Chorin A. J.,** A numerical method for solving incompressible viscous flow problems, J. Comput. Phys. 2 (1) (1967) 12–26.

21. **Travin A., Shur M, Strelets M., Spalart P.,** Physical and numerical upgrades in the Detached-Eddy Simulation of complex turbulent flows, Adv. LES of Complex Flows. 65 (Jan) (2002) 239–254.

22. **Kim S.-E., Makarov B.,** An implicit fractional-step method for efficient transient simulation of incompressible flows, Proc. 17th AIAA Comput. Fluid Dyn. Conf. June 6–9, 2005. Toronto, Ontario, Canada: American Institute of Aeronautics and Astronautics (AIAA) (2005) 2005-5253.

23. **Delany N. K., Sorensen N. E.,** Low-speed drag of cylinders of various shapes, NACA Tech. Rep. 1953. (Nov., 1) (1953) TN3038 (24 p.)

24. **Achenbach E., Heinecke E.,** On vortex shedding from smooth and rough cylinders in the range of Reynolds numbers 6×10^3 to 5×10^6, J. Fluid Mech. 109 (Aug) (1981) 239–251.

25. **Vaz G., Mabilat C., van der Wal R., Gallagher P.,** Viscous flow computations on smooth cylinders: A detailed numerical study with validation, Proc. 26-th Int. Conf. Offshore Mechanics and Arctic Engineering (OMAE-2007), June 10–15, 2007. San Diego, California, USA. Vol. 3: Pipeline and Riser Technology; CFD and VIV, ASME (2007) 849–860.

26. **Stabnikov A. S., Garbaruk A. V., Strelets M. Kh.,** Numerical simulation of the drag crisis on a sphere using a scale-resolving approach, Fluid Dyn. 59 (3) (2024) 465–478.

27. **Swanson W. M.,** The Magnus effect: A summary of investigations to date, J. Basic Eng. 83 (3) (1961) 461–470.

СПИСОК ЛИТЕРАТУРЫ

1. **Spalart P. R., Deck S., Shur M. L., Squires K. D., Strelets M. Kh., Travin A.** A new version of detached-eddy simulation, resistant to ambiguous grid densities // Theoretical. Computational and Fluid Dynamics. 2006. Vol. 20. No. 3. Pp. 181–195.

2. **Стабников А. С., Гарбарук А. В.** Алгебраическая модель ламинарно-турбулентного перехода для расчета турбулентных течений на основе метода моделирования отсоединенных вихрей // Научно-технические ведомости СПбГПУ. Физико-математические науки. 2022. Т. 15. № 1. С 16–29.

3. **Sшrensen N. N., Bechmann A., Zahle F.** 3D CFD computations of transitional flows using DES and a correlation based transition model // Wind Energy. 2011. Vol. 14. No. 1. Pp. 77–90.

4. **Hodara J., Smith M. J.** Improved turbulence and transition closures for separated flows // Proceedings of the 41st European Rotorcraft Forum (ERF2015-113). 1-st–4-th September, Munich, Germany, 2015. P. 18.

5. **Kim H. J., Kwon O. J.** Numerical simulation of transitional flows using a blended IDDES and correlation-based transition model // Computers and Fluids. 2021. Vol. 222. 30 May. P. 104916.

6. **You J. Y., Kwon O. J.** A blended model for simulating massive flow separation and laminar-turbulence transition // Proceedings of the 42nd AIAA Fluid Dynamics Conference and Exhibit. 25–28 June, 2012. New Orleans, Louisiana, USA: American Institute of Aeronautics and Astronautics (AIAA), 2012. P. 2971.

7. **Sa J. H., Park S. H., Kim C. J., Park J. K.** Low-Reynolds number flow computation for eppler 387 wing using hybrid DES/transition model // Journal of Mechanical Science and Technology. 2015. Vol. 29. No. 5. Pp. 1837–1847.

8. **Coder J. G., Ortiz-Melendez H. D.** Transitional delayed detached-eddy simulation of multielement high-lift airfoils // Journal of Aircraft. 2019. Vol. 56. No. 4. Pp. 1303–1312.

9. **Menter F. R., Matyushenko A., Lechner R., Stabnikov A., Garbaruk A.** An algebraic LCTM model for laminar–turbulent transition prediction // Flow, Turbulence and Combustion. 2022. Vol. 109. No. 4. Pp. 841–869.

10. **Menter F. R., Kuntz M., Langtry R.** Ten years of industrial experience with the SST turbulence model // Heat and Mass Transfer. 2003. Vol. 4. January. Pp. 1–9.

11. **Probst A.**, **Schwamborn D., Garbaruk A., Guseva E., Shur M., Strelets M., Travin A.** Evaluation of grey area mitigation tools within zonal and non-zonal RANS-LES approaches in flows with pressure induced separation // International Journal of Heat and Fluid Flow. 2017. Vol. 68. December. Pp. 237–247.

12. **Schewe G., van Hinsberg N. P., Jacobs M.** Investigation of the steady and unsteady forces acting on a pair of circular cylinders in crossflow up to ultra-high Reynolds numbers // Experiments in Fluids. 2021. Vol. 62. No. 8. P. 176.

13. **Menter F. R.** Two-equation eddy-viscosity turbulence models for engineering applications // AIAA Journal. 1994. Vol. 32. No. 8. Pp. 1598–1605.

14. **Schewe G.** On the force fluctuations acting on a circular cylinder in crossflow from subcritical up to transcritical Reynolds numbers // Journal of Fluid Mechanics. 1983. Vol. 133. August. Pp. 265–285.

15. **Zheng Z., Lei J., Wu X.** Numerical simulation of the negative Magnus effect of a two-dimensional spinning circular cylinder // Flow, Turbulence and Combustion. 2017. Vol. 98. No. 1. Pp. 109–130.

16. **Pereira F. S., Vaz G., Eça L.** An assessment of Scale-Resolving Simulation models for the flow around a circular cylinder // Proceedings of the Eighth International Symposium on Turbulence Heat and Mass Transfer (THMT-15). 14-th September, 2015. Sarajevo, Bosnia and Herzegovina: Begell House (USA), 2015. Pp. 295–298.

17. **Pereira F. S., Vaz G., Eça L.** Flow past a circular cylinder: A comparison between RANS and hybrid turbulence models for a low Reynolds number // Proceedings of the ASME 2015 34th International Conference on Ocean, Offshore and Arctic Engineering. Vol. 2: CFD and VIV. May 31–June 5, 2015. St. John's, Newfoundland, Canada: ASME, 2015. P. V002T08A006.

18. **Shur M., Strelets M., Travin A.** High-order implicit multi-block Navier–Stokes code: Ten-year's experience of application to RANS/DES/LES/DNS of turbulent flows (Invited lecture) // Proceedings of the 7th Symposium on Overset Composite Grids and Solution Technology. October 5–7, 2004. Huntington Beach, USA. 2004. https://cfd.spb.ru/agarbaruk/doc/NTS_code.pdf

19. **Rogers S., Kwak D.** An upwind differencing scheme for the time-accurate incompressible Navier–Stokes equations // Proceedings of the 6th Applied Aerodynamics Conference. June 06–08, 1988. Williamsburg, USA.: American Institute of Aeronautics and Astronautics (AIAA), 1988. P. 88-2583-CP.

20. **Chorin A. J.** A numerical method for solving incompressible viscous flow problems // Journal of Computational Physics. 1967. Vol. 2. No. 1. Pp. 12–26.

21. **Travin A., Shur M, Strelets M., Spalart Ph.** Physical and numerical upgrades in the Detached-Eddy Simulation of complex turbulent flows // Advances in LES of Complex Flows. 2002. Vol. 65. January. Pp. 239–254.

22. **Kim S.-E., Makarov B.** An implicit fractional-step method for efficient transient simulation of incompressible flows // Proceedings of the 17th AIAA Computational Fluid Dynamics Conference. June 6–9, 2005. Toronto, Ontario, Canada: American Institute of Aeronautics and Astronautics (AIAA), 2005. P. 2005-5253.

23. **Delany N. K., Sorensen N. E.** Low-speed drag of cylinders of various shapes // NACA Technical Reports. 1953. November 1. P. TN3038 (24 p.)

24. **Achenbach E., Heinecke E**. On vortex shedding from smooth and rough cylinders in the range of Reynolds numbers 6×10^3 to 5×10^6 // Journal of Fluid Mechanics. 1981. Vol. 109. August. Pp. 239–251.

25. **Vaz G., Mabilat C., van der Wal R., Gallagher P.** Viscous flow computations on smooth cylinders: A detailed numerical study with validation // Proceedings of the 26-th International Conference on Offshore Mechanics and Arctic Engineering (OMAE-2007). June 10–15, 2007. San Diego, California, USA. Vol. 3: Pipeline and Riser Technology; CFD and VIV. ASME, 2007. Pp. 849–860.

26. **Stabnikov A. S., Garbaruk A. V., Strelets M. Kh.** Numerical simulation of the drag crisis on a sphere using a scale-resolving approach // Fluid Dynamics. 2024. Vol. 59. No. 3. Pp. 465–478.

27. **Swanson W. M.** The Magnus effect: A summary of investigations to date // Journal of Basic Engineering. 1961. Vol. 83. No. 3. Pp. 461–470.

THE AUTHORS

STABNIKOV Andrey S.
Peter the Great St. Petersburg Polytechnic University
29 Politechnicheskaya St., St. Petersburg, 195251, Russia
an.stabnikov@gmail.com
ORCID: 0000-0001-7011-6197

GARBARUK Andrey V.
Peter the Great St. Petersburg Polytechnic University
29 Politechnicheskaya St., St. Petersburg, 195251, Russia
agarbaruk@mail.ru
ORCID: 0000-0002-2775-9864

СВЕДЕНИЯ ОБ АВТОРАХ

СТАБНИКОВ Андрей Сергеевич – *аспирант Высшей школы прикладной математики и вычислительной физики Санкт-Петербургского политехнического университета Петра Великого.*
195251, Россия, г. Санкт-Петербург, Политехническая ул., 29
an.stabnikov@gmail.com
ORCID: 0000-0001-7011-6197

ГАРБАРУК Андрей Викторович – *доктор физико-математических наук, доцент Высшей школы прикладной математики и вычислительной физики Санкт-Петербургского политехнического университета Петра Великого.*
195251, Россия, г. Санкт-Петербург, Политехническая ул., 29
agarbaruk@mail.ru
ORCID: 0000-0002-2775-9864

Received 27.08.2024. Approved after reviewing 28.10.2024. Accepted 29.10.2024.
Статья поступила в редакцию 27.08.2024. Одобрена после рецензирования 28.10.2024. Принята 29.10.2024.